Proposal for kf effective notch factor estimation for life assessment of welded joint based on geometric parameters

Engineering Failure Analysis 157 (2024) 107944

Contents lists available at ScienceDirect

Engineering Failure Analysis

journal homepage: www.elsevier.com/locate/engfailanal

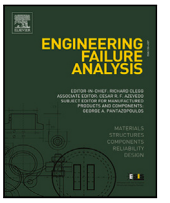

Proposal for k_f effective notch factor estimation for life assessment of welded joint based on geometric parameters

Raffaella Sesana, Luca Santoro *

Dipartimento di Ingegneria Meccanica e Aerospaziale - Politecnico di Torino, Corso Duca degli Abruzzi 24, Torino, 10129, Italy

ARTICLE INFO

Keywords:
Weldings
Fatigue
Geometric parameters
Notch factor

ABSTRACT

Mechanical joining techniques are fundamental in the industrial landscape, with welded joints standing out as a primary method across diverse manufacturing sectors. In this work, we present a novel contribution to fatigue life assessment of welds through 3D-Scanning of weld seam. The methodology is applied on welded specimens tested in alternate bending fatigue, showing that for real case applications, statistical approach to surface irregularities of the joint plays a keyrole. In particular by means of surface scanning, some statistical geometric parameters are obtained to characterize the weld seam. Then by experimental fatigue testing a relation between geometrical measured parameters, experimental cycles to failure and crack nucleation sites is obtained. Then FEM models generated basing on 3d scanning are used for FEM simulations aiming at validating the stress concentration related to surface geometric irregularities and fatigue life. A dedicated software, called 3D-life, was developed to process surface scans and the results of the numerical simulation and life estimations were used to predict the crack nucleation sites.

1. Introduction

Mechanical joining techniques are fundamental in the industrial landscape, with welded joints standing out as a primary method across diverse manufacturing sectors. Their ubiquity underscores the need for continuous research and optimization.

The welding process, while indispensable, is inherently intricate. Achieving consistent mechanical properties amidst this complexity remains a challenge. Today, a vast array of alloys can be welded, but steel, particularly the S275 mild steel, is a mainstay in industrial applications. The mechanical attributes of S275 are well-documented, as highlighted in [1]. However, welding can introduce a metallurgical notch effect due to microstructural alterations [2]. With the right parameters, it is possible to minimize common defects such as porosities and lack of wall fusion [3–7]. Moreover, despite the presence of the heat-affected zone and residual stresses [8,9], the overall mechanical integrity of the joint typically remains uncompromised [10,11].

Welding versatility is evident in its adoption across diverse industries, from oil and gas to automotive and railways. In applications where the weld geometric appeal is paramount, such as in cars or trains, the welds are often externally visible. These welds, termed 'aesthetical welds', might undergo processes like milling or 'dressing' to enhance their appearance, though this comes at an added cost. Beyond aesthetics, this milling process can enhance the joint mechanical properties [12–14], especially when considering the significant role surface defects play in fatigue analyses [15–17]. Given that real-world loading conditions often involve bending or multiaxial stresses [18], ensuring the surface integrity becomes even more critical, especially for thicker components. So, the bead geometrical parameters plays a crucial role in fatigue design of weld joint [19]. Due to the technology itself, the welded joint [20] has to be fatigue designed and then tested in order to assess welding defects.

* Corresponding author.
E-mail addresses: raffaella.sesana@polito.it (R. Sesana), luca.santoro@polito.it (L. Santoro).

https://doi.org/10.1016/j.engfailanal.2023.107944
Received 5 November 2023; Received in revised form 18 December 2023; Accepted 28 December 2023
Available online 30 December 2023

Nomenclature

α_e	dihedral angle of two faces meeting at edge e
β	Neuber constant
$\lambda_{inf}, \lambda_{sup}, \lambda_{inf,gauss}, \lambda_{sup,gauss}$	inferior and superior limit threshold for minimum, maximum,
σ	mechanical stress [MPa]
σ_{D-1}	fatigue limit at R=-1
σ_{vm}	simulated von Mises equivalent stress
τ	shear stress
θ_f	interior angle of face f [rad]
A_f	Area of a facet f $[m^2]$
$Area_{bead}$	surface area of the weld bead
$Area_{tot}$	total surface area of the specimen
b	support distance
DI	damage index [m]
e	identifier of an edge
F	force applied by the testing machine
F_a	force amplitude
f	unique face of the triangulation **T**
$F_{\mathbf{v}}$	set of facets meeting at vertex **v**
FSF	fatigue safety factor
GMAW	gas metal arc welding
HAZ	heat affected zone
H_e	curvature of an edge e [1/m]
$\overline{H_e}$	average of the curvature over an edge neighbor e [1/m]
$H_{\mathbf{v}}$	average curvature of a vertex **v**
k_f	effective fatigue notch factor
k_t	stress concentration factor
$K_{\mathbf{v}}$	Gaussian curvature $[1/m^2]$
$\kappa_{\mathbf{v},min}$	minimum curvature of a vertex **v**
$\kappa_{\mathbf{v},max}$	maximum curvature of a vertex **v**
l_e	length of an edge e
M	bending moment
M	3D scan mesh
n	Neuber's constant
n	normal vector of a facet
p	percentile of vertex in the weld bead
q	fatigue notch sensitivity
R	stress ratio
RSS	residual sum of square
r	curvature radius [m]
R^2	coefficient of determination
s	thickness of the specimen
SMAW	shielded metal arc welding
T	Triangulation
$\lvert\mathbf{v}\rvert$	total number of vertex in the scan
v	vertex of a triangle
w	width of the specimen
W_f	section modulus
y	generic variable studied during fitting procedure

The research landscape in fatigue design domain is wide. A significant portion focuses on the stress intensification effects due to the geometrical complexity of the weld toe, especially in T-joint or K-joint weld beads [21–25]. This approach is also evident in butt joints [26,27]. In these situations, fatigue damage often originates at the weld toe, and statistical analysis on macro-sections can be

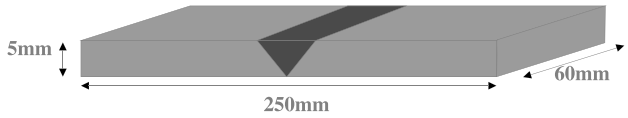

Fig. 1. Specimen.

Table 1
Chemical composition (%wt) of S275JR steel.

C%	Mn%	P%	S%	N%	Cu%
0.21	1.5	0.035	0.035	0.012	0.55

applied in order to assess the weld toe angle [28,29]. Automated methods, such as the one proposed in [30], offer a simulation-based assessment of these joints based on the peak stress method [26,31–34]. Another widely adopted methodology is the theory of critical distances [35], which, besides welding, finds applications in additive manufacturing [21,36–45].

However, automated welding processes offer consistency to these approaches as the welded surface is smoother and more regular. On the other hand, manual weld bead can be more variable. Factors like torch position or weld groove preparation can introduce irregularities, leading to unevenly distributed defects along the joint. This variability underscores the need for comprehensive quality assessments, as a single section might not fully represent the joint's quality. Although there are weld quality standards [46], as reviewed in [47], a universally accepted fatigue criteria for weld defects remains elusive relating to both internal and superficial defects.

Given this backdrop, 3D scanning of weld bead emerges as a pivotal tool, enhancing quality inspection [48]. It has been leveraged to explore various facets of welding, from studying corrosion effects [49] to developing methods for measuring weld angles and radii [50,51]. The significance of a statistical approach in actual applications is further emphasized in [52]. The methodology is based on the experimental hypothesis that there is a relationship between the geometric parameters and the initiation of the fatigue crack and therefore on the fatigue life. Among the geometric parameters, in this paper we considered the local curvature of the weld bead surface. In general, macroscopic geometric irregularities are described by material and geometric parameters such as k_t, stress concentration factor [53], and k_f, fatigue notch factor [53], which describe their effect in terms of overstress and damage effect. In particular the stress concentration factor is related to the effect of the irregularities on the actual stress distribution and how the curvature and the dimension of the irregularities can affect the multiaxiality of the stress. On the other hand, the fatigue notch factor k_f is related to the estimation of this irregularities on fatigue life. For a highly irregular surface such as that of a weld, each irregularity constitutes a notch. Each notch has both a local and global effect, as the number of notches influences the number of cracks triggered. Therefore, the global reduction in fatigue life, has an effect on the overall fatigue behavior of the welding. For this purpose, a global and statistical approach to quantify the effect of irregularities is required on one hand. On the other hand, a description of each individual welding surface is required. In this work, some possible risk indices of fatigue crack initiation in welded surfaces are proposed and investigated, based on the surface morphology and therefore linked to the geometric welding parameters. They are parameters which can be obtained by simple and economical procedures and starting from scans of the weld surfaces. These parameters allow quantifying in detail the risk index of each individual weld.

In the present paper the influence of geometric defects in fatigue life of manual welding is investigated. This paper introduces a novel contribution to the 3D scanning fatigue life assessment domain. In particular we present an empirical estimation method of the weld fatigue notch factor k_f hereon called effective notch factor related to geometric defects, designed to bypass simulations, aiming at streamlined result interpretation and industrial applicability.

2. Materials

This work investigates the fatigue behavior of carbon-steel manually-welded joints. To this aim, the plate welds were executed using two distinct welding methods. The first method was Shielded Metal Arc Welding (SMAW), a traditional approach. The second method employed was Gas Metal Arc Welding (GMAW), which is often referred to as GMAW (Metal-arc Inert Gas) or MAG (Metal-arc Active Gas) welding. This latter method embodies a more complex welding process. The specimens used for laboratory tests are obtained from welded plates, 5 mm thick. Seven specimens were extracted (4 GMAW and 3 SMAW), 60 mm in width and a length of 250 mm, compatible with the testing equipment (see Fig. 1).

The specimens are composed of S275JR steel (Yield stress 275 MPa). Chemical composition is reported in Table 1. Material alternating fatigue limit (R=−1), is 160 MPa [1].

The welding system is *TECNOWELD MIG 110, 35–100 A, 0.6–0.8 mm* and *AWELCO ARC 250*, while the consumable used for SMAW technique is *Oerlikon TENAX 35S* of $\phi = 2$ mm. The specimens were obtained by means of setting the optimal welding parameters for each welding technique, presented in Table 2.

The micrographic analysis of welding cross-section was performed by means of*Nital 3%* chemical etching; microhardness measurements were run by means of *Innovatest Nova 130* microhardness testing equipment, according to [54]. In Fig. 2(a) a pearlitic-ferritic microstructure is evident for base material, Fig. 2(b) shows a lower bainite microstructure for SMAW weld bead, and in Fig. 2(c) a bainitic microstructure with large martensite isle is present for GMAW weld bead. The measured hardnesses are 120HV1 for the base material, 150HV1 for the SMAW weld bead, and 190HV1 for the GMAW weld bead.

Table 2
Optimal welding parameter.

	Voltage	Current	Power	Travel speed	Heat input
SMAW	18 V	95 A	1700 W	2 mm/s	850 J/mm
GMAW	25 V	50 A	1250 W	2 mm/s	625 J/mm

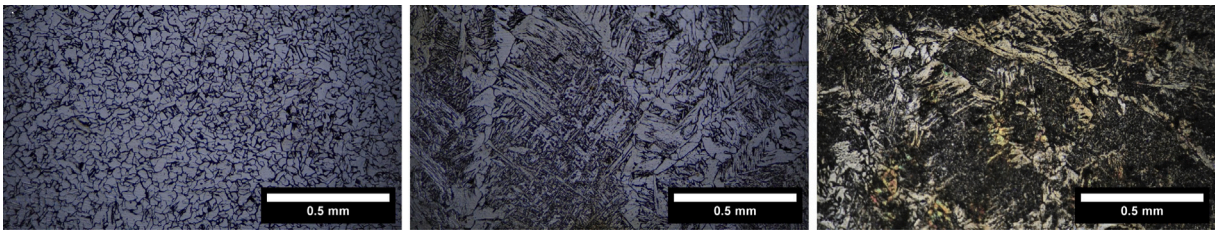

(a) Base Material (b) SMAW - weld bead (c) GMAW - weld bead

Fig. 2. Microstructures.

3. Methods

This work was developed starting from some welds performed on flat plates described in the materials section. To quantitatively describe the specific irregularities of each weld and obtain descriptive parameters of fatigue behavior, the activity was carried out in 4 phases.

- In the first phase, the surfaces of each individual weld were scanned. The scan data were then processed and the results displayed. In particular, data processing focused on surface curvature definition and measurement.
- In the second phase, symmetrical alternating 4-point flexural fatigue tests were performed to find the fatigue strength at 1 million cycles and the crack initiation points.
- In the third phase, static structural simulations were performed for each specimen, characterized by its specific geometric parameters, to obtain the local stress concentration factor k_t and Fatigue Safety Factor (FSF, see Section 3.3) value on the surface of the bead.
- In the fourth and last phase, an empirical model relating the curvature parameters and the fatigue strength at 1Mln of cycles [53] of the specimens is calibrated and validated. Furthermore, the values of the curvature parameters obtained in phase 1 and the simulations obtained in phase 3 were compared with the results of the experimental tests obtained in phase 2 in order to study their influence on the mechanical behavior of the joint and point out a possible correlation. Furthermore, the fatigue crack initiation points obtained in phase 2 were compared with the areas with FSF lower than 1 obtained by numerical simulations and with metrics lower than a threshold obtained in phase 3.

3.1. Surface acquisition and processing

The specimens were scanned by a *CreaForm Go!Scan Spark* with an accuracy of 0.05 mm and a texture resolution of 200DPI.

The core data for this investigation is sourced from a set of STL (Stereolithography) files which depict three-dimensional scans of welded specimens. STL, a widely accepted format, stores three-dimensional models as raw triangulated surfaces. An STL file comprises a series of triangular facets, each defined by its vertices and a unit normal vector (see Fig. 3). Mathematically, a triangular facet is represented as:

$$\mathbf{T} = \left\{\mathbf{v}_1, \mathbf{v}_2, \mathbf{v}_3; \mathbf{n}\right\}, \tag{1}$$

where $\mathbf{v}_1, \mathbf{v}_2, \mathbf{v}_3$ are the vertices of the triangle, and $\mathbf{n}$ is the unit normal vector to the triangle plane. The triangulation T consists of $|\mathbf{v}|$ unique vertices. The normal vector $\mathbf{n}$ can be computed as:

$$\mathbf{n} = \frac{\left(\mathbf{v}_2 - \mathbf{v}_1\right) \times \left(\mathbf{v}_3 - \mathbf{v}_1\right)}{\left\| \left(\mathbf{v}_2 - \mathbf{v}_1\right) \times \left(\mathbf{v}_3 - \mathbf{v}_1\right) \right\|}. \tag{2}$$

Upon importing the STL files, the data undergo processing to extract the essential geometric and topological features, laying the groundwork for subsequent curvature calculations.

A subsequent action of mesh cleaning is required to purge the mesh of any redundancies. Specifically, it identifies and eliminates duplicate points, unused points or cells that might be lingering in the mesh structure. This cleaning process does not refine or alter the mesh quality or resolution. Mathematically, the cleaning process can be visualized as a transformation:

$$\mathbf{M}_{\text{raw}} \rightarrow \mathbf{M}_{\text{clean}}, \tag{3}$$

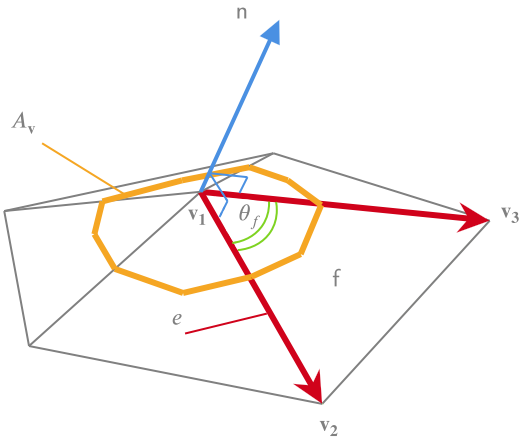

Fig. 3. Scheme of triangulation definitions.

where $\mathbf{M}_{\text{raw}}$ signifies the initial, unprocessed mesh, and $\mathbf{M}_{\text{clean}}$ denotes the cleaned, non-redundant mesh. This cleaned representation, $\mathbf{M}_{\text{clean}}$, forms the basis for all ensuing computations.

3.1.1. Curvature computation and range definition

The Discrete Gauss curvature in the generic vertex $\mathbf{v}$ (K_v) is given by:

$$K_{\mathbf{v}} = \frac{1}{A_{\mathbf{v}}}\left(2\pi - \sum_{f \in F_{\mathbf{v}}} \theta_f\right) \tag{4}$$

where:

- $K_{\mathbf{v}}$ is the Gaussian curvature at vertex $\mathbf{v}$.
- $F_{\mathbf{v}}$ is the set of faces that meet at vertex $\mathbf{v}$.
- θ_f is the interior angle of face f at vertex $\mathbf{v}$.
- $A_{\mathbf{v}}$ is the area associated with the vertex $\mathbf{v}$

The contribution of every facet is weighted by the facet area A_f by 3, so $\frac{A_f}{3} = \frac{1}{2} * \frac{1}{3} * \|(\mathbf{v}_2 - \mathbf{v}_1) \times (\mathbf{v}_3 - \mathbf{v}_1)\|$. The units of Gaussian Curvature are m^{-2}. So that, $A_{\mathbf{v}} = \sum_{f \in F_{\mathbf{v}}} \frac{A_f}{3}$

The Mean Curvature of a vertex $\mathbf{v}$ can be defined as follows. Let $\overline{H_e}$ be the average over the edge neighbors of H_e:

$$H_e = l_e \times \alpha_e \tag{5}$$

where e is an edge, l_e is the length of the edge e and α_e is the dihedral angle between the two facets meeting at edge e such that $-\pi < \alpha_e < \pi$.

Then $H_{\mathbf{v}}$ is defined as:

$$H_{\mathbf{v}} = \overline{H_e}. \tag{6}$$

This means that the surface is assumed to be orientable and the computation creates the orientation. The units of Mean Curvature are m^{-1}.

The Maximum ($\kappa_{\mathbf{v},\max}$) and Minimum ($\kappa_{\mathbf{v},\min}$) Principal Curvatures are given by:

$$\kappa_{\mathbf{v},\max} = H_{\mathbf{v}} + \sqrt{H_{\mathbf{v}}^2 - K_{\mathbf{v}}}, \tag{7}$$

$$\kappa_{\mathbf{v},\min} = H_{\mathbf{v}} - \sqrt{H_{\mathbf{v}}^2 - K_{\mathbf{v}}}. \tag{8}$$

Excepting spherical and planar surfaces which have the same principal curvatures, the curvature at a point on a surface varies with the direction one "sets off" from the point. For all directions, the curvature will pass through two extrema: a minimum ($\kappa_{\mathbf{v},\min}$) and a maximum ($\kappa_{\mathbf{v},\max}$) which occur at mutually orthogonal directions to each other.

For what concerns the signs of the curvatures, the sign of the Gauss Curvature is a geometric invariant; it should be positive when the surface looks like a sphere, negative when it looks like a saddle. However, the sign of the Mean Curvature depends on the convention for normals. This code assumes that normals point outwards (i.e., from the surface of a sphere outwards).

Therefore it is necessary to define a threshold on curvature value to be considered in our calculations. To this aim a preliminary study has been conducted in order to find a threshold value which might discretize whether a n irregularity on the surface can be

considered a notch or not. Under the assumption that all the notches are in the weld bead, and under the hypothesis that the scan texture is uniform, it can be said that the number of vertex of the scan inside the weld bead is $|\mathbf{v}| \times \frac{Area_{bead}}{Area_{tot}}$, where $|\mathbf{v}|$ is the total number of vertex in the scan. The total Area $Area_{tot}$ is defined as $Area_{tot} = 250 \times 5 \times 60 = 75000mm^2$, while the $Area_{bead}$ for a 45° groove is defined as $Area_{bead} = 5 * 2 * 60 = 600mm^2$. We can define a value $p = \frac{Area_{bead}}{Area_{tot}} \times 100$. Then the assumption that all the notches ($k_{\mathbf{v}}, K_{\mathbf{v}}, H_{\mathbf{v}} < 0$) are inside the weld bead we could say that the p_{th} percentile of vertex surely contain all the notches. In fact, all the notches have negative curvature and so the p_{th} percentile of the curvature ($1/r$) contains the information about the notches. This information has been used to define a threshold for the data to be evaluated. So, the right limit of the p_{th} percentile of the curvature values has been evaluated for all the tests. All these values lay around −0.6 [1/mm], so a unique value is chosen as the threshold. Defining the limits symbolically:

$\lambda_{\text{inf}} = -100$

$\lambda_{\text{sup}} = -0.6$

$\lambda_{\text{inf, gauss}} = -\lambda_{\text{inf}}^2$

$\lambda_{\text{sup, gauss}} = -\lambda_{\text{sup}}^2$

The valid ranges for Mean, Maximum, and Minimum Curvatures are:

$$\lambda_{\text{inf}} \leq \kappa_{\mathbf{v}} \leq \lambda_{\text{sup}}, \tag{9}$$

and for Gaussian Curvature:

$$\lambda_{\text{inf, gauss}} \leq K_{\mathbf{v}} \leq \lambda_{\text{sup, gauss}}. \tag{10}$$

The Radii of Curvature r_{type} are defined related to each curvature definition:

$$r_{type} = \begin{cases} -\frac{1}{\overline{\kappa_{\mathbf{v}}}} & \text{for } \kappa_{\mathbf{v}} \in \{H, \kappa_{\text{v,max}}, \kappa_{\text{v,min}}\}, \\ \frac{1}{\sqrt{|\overline{K_{\mathbf{v}}}|}} & \text{for } K_{\mathbf{v}}, \end{cases} \tag{11}$$

where the $\overline{\kappa_{\mathbf{v}}}$, and $\overline{K_{\mathbf{v}}}$ are the arithmetic average of respectively $\kappa_{\mathbf{v}}$ and $K_{\mathbf{v}}$.

Finally, the Damage Index Calculation DI_{type} is again defined according to the curvature definition:

$$DI_{\text{type}} = \frac{-1}{\sum \kappa}. \tag{12}$$

The summation is over curvature values within the specified limits λ_{inf} and λ_{sup}.

3.1.2. Visualization

In the context of our study, where the irregular and complex geometry of welded joints is distilled into numerical curvatures, graphical representations of parameters become indispensable.

The primary tool employed for this purpose is the histogram. Each bar in a histogram represents the tabulated frequency at each interval, making it an effective tool for understanding the distribution of curvature values.

For the computed curvature values, as an example,histograms are plotted (Fig. 4) to provide insights into: spread, skewness, outliers.

As regards spread, the range covered by the histogram bars indicates the variation in curvature values. This information is crucial to quantify the ranges of notches radius.

For the skewness, the asymmetry or symmetry of the histogram reveals whether the curvature values have a particular direction of skewness. It is possible to comprehend the concentration of flaws that have the same curvature.

Regarding the outliers, any bars that are detached from the main body of the histogram might indicate outlier values that are significantly different from the rest.

3.1.3. Dataset segregation and mathematical modeling

The dataset is categorically divided based on the welding techniques employed: GMAW and SMAW. Owing to the inherent differences between these techniques, it is paramount to analyze them separately. Their distinct characteristics might have specific influences on the curvature values and the ensuing mathematical modeling. For each subset, the focal point of the mathematical model is the hyperbolic relationship [55]:

$$y(\sigma_{d-1}) = 1 + \left(\frac{1}{\sigma_{d-1}}\right)^a. \tag{13}$$

Here, σ_{d-1} represents the fatigue limit specific of each welded specimen, serving as the independent variable. The parameter a is optimized to fit the data most aptly. The non-linear least squares method, employed for this optimization, aims at minimizing the residual sum of squares RSS:

$$RSS = \sum_{i=1}^{n} \left(y_i - y(\sigma_{d-1,i})\right)^2, \tag{14}$$

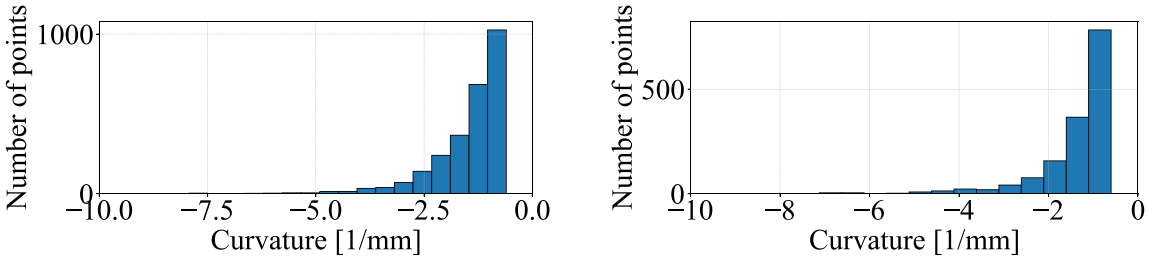

Fig. 4. Histograms representing the minimum curvature κ_{min} distribution of the points with negative curvature of specimen 1(a) and specimen 3(b).

where n is the number of data points, y_i are the observed values, and $y(\sigma_{d-1,i})$ are the values predicted by the model.

The efficacy of the model in capturing the underlying data trend is quantified using the coefficient of determination, R^2:

$$R^2 = 1 - \frac{\sum_{i=1}^{n} \left(y_i - y(\sigma_{d-1,i})\right)^2}{\sum_{i=1}^{n} \left(y_i - \bar{y}\right)^2}. \tag{15}$$

In this formula, $\bar{y}$ designates the mean of the observed values. An R^2 value nearing 1 is indicative of an excellent model fit. Upon completing the mathematical modeling, the results, encompassing graphical plots and optimized parameters pertinent to both GMAW and SMAW techniques, are systematically stored thanks to our 'in-house' software *3D-Life* which automatizes this process.

3.2. Fatigue test

An Amsler HFP 100 resonating testing machine was utilized for alternating bending fatigue tests. The specimens underwent a four-point bending test (Fig. 5), with support distance $b = 26$ mm. The weld bead has been placed inside the zone of constant bending moment. Each specimen was subjected to a sequence of loading blocks (1 million cycles) with increasing stress amplitude and constant stress ratio $\frac{\sigma_{min}}{\sigma_{max}} = -1$ until failure. In Fig. 6 an example of the load history is provided in order to better clarify the testing methodology. This procedure aims to discern the stress level at which the specimen will fail, thereby determining the real σ_{D-1} — the stress limit allowing the specimen to achieve infinite life.

For each loading level, the maximum bending moment M_{max} is:

$$M_{max} = b \times \frac{F}{2}, \tag{16}$$

where F is the force applied by the testing machine.

Given the rectangular cross-section of the specimen, the nominal maximum stresses can be deduced using:

$$\sigma_{\max} = \frac{M_{max}}{W_f}, \tag{17}$$

where W_f is the section modulus.

The section modulus W_f, dependent on the specimen shape, can be calculated as:

$$W_f = \frac{w \times s^2}{6}, \tag{18}$$

where w is the specimen cross-sectional width, and s is its thickness.

Initially, a low bending force amplitude (F_a) of 400 N is applied to the specimen. This force is incrementally enhanced by 200 N after every 10^6 cycles. When the specimen fails, the nominal maximum stress in the weld bead corresponding to the last loading block is assumed as experimental $\sigma_{\text{D-1}}$. This value is expected to change for each specimen as the surface morphology of each weld bead differs for each specimen. Accordingly, the k_f of each specimen is then calculated as the ratio between the material fatigue limit (160 MPa) and the fatigue limit $\sigma_{\text{D-1}}$ of each specimen.

$$k_f = \frac{\sigma_{\text{D-1}}}{160 \text{ MPa}} \tag{19}$$

The corresponding values are reported in Table 5.

3.3. Numerical model

The numerical model was developed using ANSYS Mechanical APDL 2023R2. The STL file from the scan underwent preprocessing to transform the triangulation into a parametric surface. This transformation allows the mesh to adapt to the surface curvature, ensuring that regions with higher curvature have denser mesh configurations.

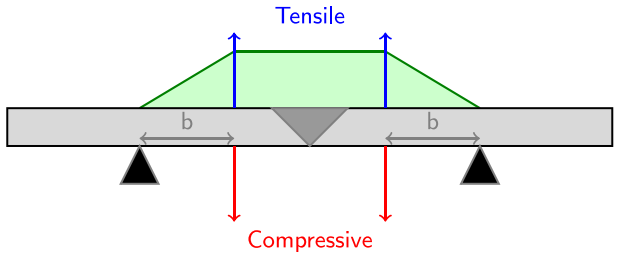

(a)

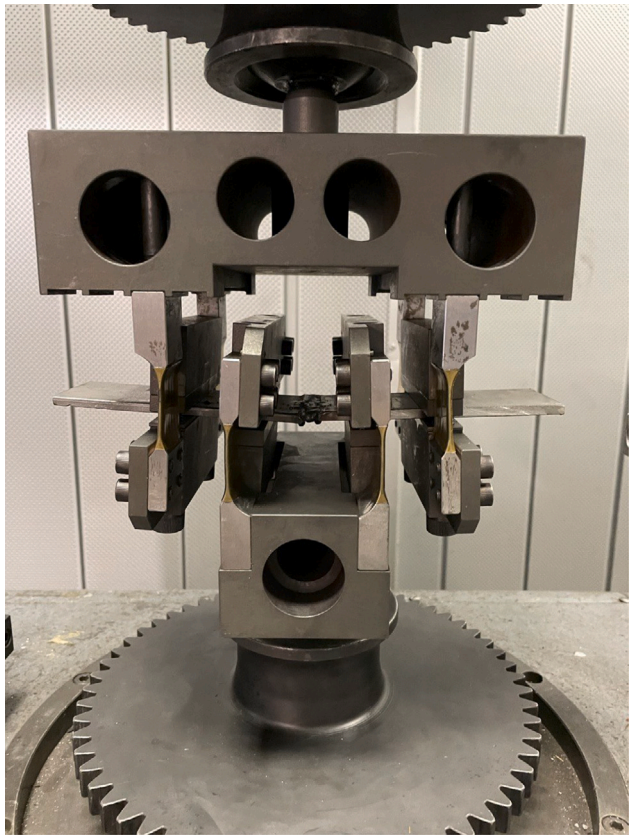

(b)

Fig. 5. 4 Point bending test: (a) scheme and (b) testing equipment with load reversal.

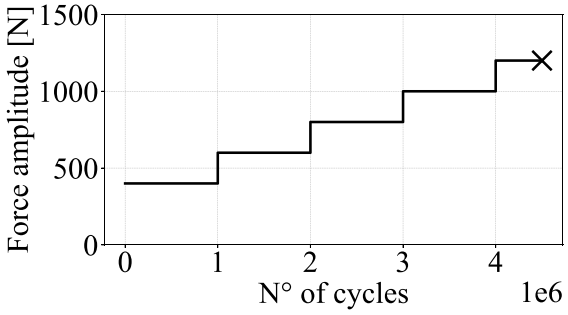

Fig. 6. Load history example.

Table 3
Fatigue test results.

Specimen no.	Type	Nominal σ_{d-1}	Cycles no. last step
1	GMAW	83.2	48 847
2	SMAW	83.2	545 232
3	SMAW	62.4	497 201
4	GMAW	78.0	977 424
5	GMAW	87.3	966 223
6	GMAW	74.88	680 006
7	SMAW	49.92	264 062

Let the mesh density function be represented as $\rho(\kappa)$, where κ is the surface curvature. In areas of pronounced curvature, $\rho(\kappa)$ increases, indicating a denser mesh.

Material constitutive model is linear elastic. The fatigue toolbox was then employed, setting the fatigue endurance at 160 MPa for 10×10^6 cycles, based on the findings of [1]. A constant bending moment, denoted as M_{max} and corresponding to the load at which each specimen failed, was applied along the longitudinal direction of the weld.

In particular the moment applied to each model, M_{max}, was chosen based on the fatigue test results, as detailed in Section 4 and Table 3.

In the post-processing phase, emphasis was placed on two outputs: the equivalent von Mises stress, σ_{vm}, and the fatigue safety factor, FSF. This factor is calculated by the solver as the ratio between the material fatigue limit and the local value of the von Mises equivalent stress. The maximum value of σ_{vm} on each simulated weld sample, $\sigma_{vm,max}$ was normalized using σ_{d-1} to compute the stress concentration factor, k_t related to each sample, as follows:

$$k_t = \frac{\sigma_{vm,max}}{\sigma_{d-1}}, \tag{20}$$

where σ_{d-1} is assumed as the nominal applied stress for the simulated sample. In Table 5 the resulting values of k_t are reported. Additionally, Biaxiality indications were retrieved and studied. it is defined as the principal stress smaller in magnitude divided by the larger principal stress, with the principal stress nearest zero ignored. A biaxiality of zero corresponds to uniaxial stress, a value of –1 corresponds to pure shear, and a value of 1 corresponds to a pure biaxial state. Biaxiality of load in fatigue life assessment of welded joints cannot be neglected, as discussed in [56].

4. Results and discussion

The experimental tests have been performed as explained in Section 3.2, therefore the maximum nominal stress amplitude σ_{d-1} applied during the step loading for each specimen is presented in Table 3. As expected, a large scatter in the fatigue endurance is present. All the specimen were fatigued along step of the same duration. So, if present, the same coaxing effect affected all of them and this could be reflected in the σ_{d-1} values.

4.1. Curvature influence in fatigue life

The experimental k_f vs each extracted curvature-based features was plotted and the data were fitted with the model described in Eq. (14) for each subset. In particular for each studied curvature, the average curvature radius and the corresponding damage index vs the experimental k_f is plotted. In Table 4 the curve fitting optimized parameters are presented with the corresponding R^2. Since the curvature values considered for this calculation were only the negative one, we could say that almost every type of curvature might contain information about notch effect.

In Figs. 7 and 11–13 these results regarding the two subsets are presented. The Average Curvature Radius value represents a quantification of the value of the investigated parameter, while the Damage Index is related to how many irregularities characterized by the investigated radius are present on the surface. For example in Fig. 6(a) the k_f vs the average radius obtained from Minimum Curvature is plotted, while in Fig. 6(b) the same plot vs the corresponding Damage Index. The Minimum radius, corresponding to maximum curvature, captures the sharpest irregularities. It can be observed that for both welding techniques the approximating curve fits the experimental data with good correlation coefficient (0,730 for GMAW and 0,996 for SMAW) thus confirming the choice of the model and the ability of the model to capture the sensitivity of this curvature parameter to welding fatigue behavior. When considering the corresponding Damage Index, it can be observed that while for SMAW samples the correlation coefficient is 0,997, for GMAW samples the correlation is less significant and R2 is 0,182. This can be due to the fact that the surfaces of the different GMAW samples shows the same degree of irregularity. On the other hand the SMAW samples result, for what concerns the Minimum Radius, with different distribution of irregularities. Similar discussion can be extended to the average radius corresponding to Gaussian Curvature (figure 9), to Maximum Curvature (figure 10) and to Mean Curvature (figure 11). For all subsets, SMAW specimen shows higher k_f with respect to GMAW specimens, and the two subsets group in different areas of the plots. Additionally the GMAW tests showed really low scatter, the point are in fact grouped in a small area, and it is consequently difficult to find a pattern, however the minimum curvature shows a clear trend both for the radius and the damage index plot, also the gaussian curvature radius plot shows a good trend. As expected, the average radius and damage index of the minimum curvature best fits the experimental data and it will be used for results discussion in the following sections.

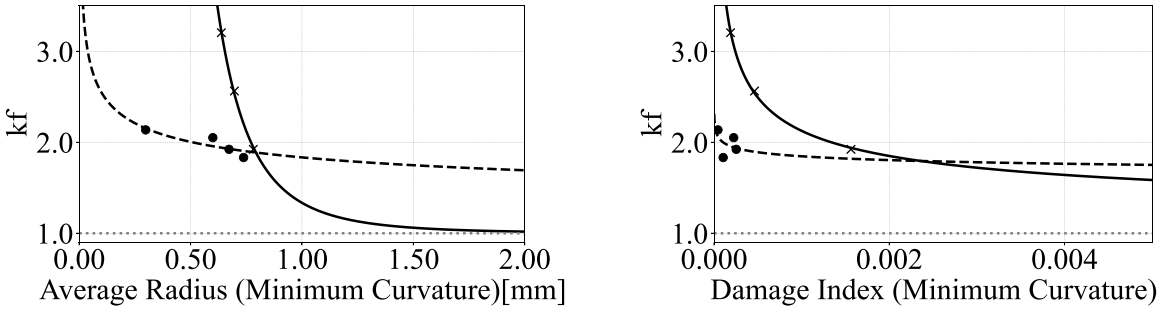

(a) radius (b) damage

Fig. 7. Experimental kf vs (a) Minimum curvature and (b) Damage Index for SMAW ('*x*', continuous fitting curve) and GMAW ('*o*', dotted fitting curve) welds.

Table 4
Fitting curve parameters for curvature-based mathematical modeling.

Parameter	Type	a	R^2
r_{mean}	GMAW	0.130	0.567
r_{mean}	SMAW	1.500	0.434
$r_{gaussian}$	GMAW	0.664	0.387
$r_{gaussian}$	SMAW	3.410	0.999
r_{max}	GMAW	0.000	0.000
r_{max}	SMAW	4.250	0.995
r_{min}	GMAW	0.269	0.730
r_{min}	SMAW	4.210	0.996
DI_{mean}	GMAW	0.088	0.352
DI_{mean}	SMAW	0.442	0.990
DI_{gauss}	GMAW	0.025	0.005
DI_{gauss}	SMAW	0.651	0.902
DI_{max}	GMAW	0.000	0.000
DI_{max}	SMAW	0.376	0.971
DI_{min}	GMAW	0.091	0.182
DI_{min}	SMAW	0.464	0.997

4.2. Numerical simulation

In Table 5, for each specimen the minimum radius (column 2), the experimental k_f (column 3) and the simulated k_t obtained according to Eq. (20) (column 4) are reported. The k_t in table is related to the point, in the weld bead where the equivalent Von Mises stress σ_{D-1} reaches the highest values, that is corresponding to the smallest $r_{v,\min}$ on the surface. In Fig. 12(b)–18(b) the red areas show the point where the curvature radius lies in the threshold range.

In Fig. 8, the k_t and k_f vs the minimum value of the minimum radius for each specimens. It is evident that the maximum equivalent von Mises stresses (related to k_t) are higher than the effective fatigue stresses (related to k_f), given the same nominal stress on the specimen. The relation between these different conditions is defined by the fatigue notch sensitivity q, and it is expressed by the formula:

$$q = \frac{k_f - 1}{k_t - 1}. \tag{21}$$

According to Neuber's equation [57], we can express q as:

$$q = \frac{1}{1 + \frac{\sqrt{\beta}}{\sqrt{r}}}, \tag{22}$$

where β is the Neuber constant and depends on the material, and r the curvature radius of the notch. This well assumed approach, documented in literature for conventional notch effect modellization, reports for a relation of k_f and k_t with the material properties and an inverse proportional relation with the square root of the notch radius. In the present case, where the notch are represented by welding irregularities, the same pattern is observed.

The local surface curvature generates a local multiaxial stress distribution. For example, in [58,59] the effect of the curvature radius concerning the angle with the load was deeply studied. The stress biaxiality indication map of specimen 1 is presented in Fig. 9 as an example. Referring to [56] a critical value for the biaxiality stress ratio (σ/τ) is 1, so when the normal stress is equal or lower with respect to the shear stress (45 degree angle of the defect with respect to the load direction) the biaxiality is not negligible

Table 5
Simulated stress concentration factor k_t and experimental effective fatigue notch factor k_f for investigated specimens.

Specimen no.	min(r_{min})	k_f	k_t simulated
1	0.045	1.9	4.0
2	0.235	1.9	2.5
3	0.039	2.5	5.0
4	0.050	2.1	5.1
5	0.061	1.8	2.4
6	0.036	2.1	4.0
7	0.083	3.2	2.5

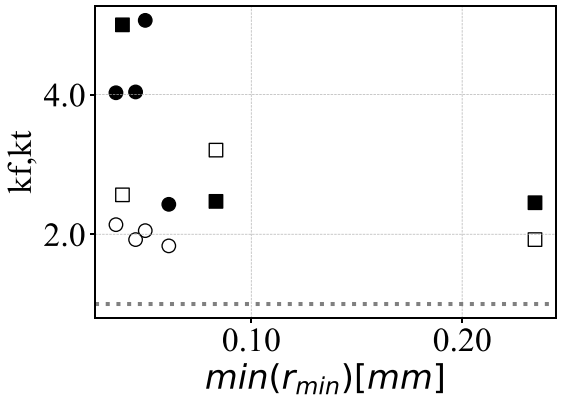

Fig. 8. Overview on $kt_{simulated}$ (full markers) vs r_{min}, and k_f (empty markers) vs r_{min}, for SMAW (square) and GMAW (round) specimens.

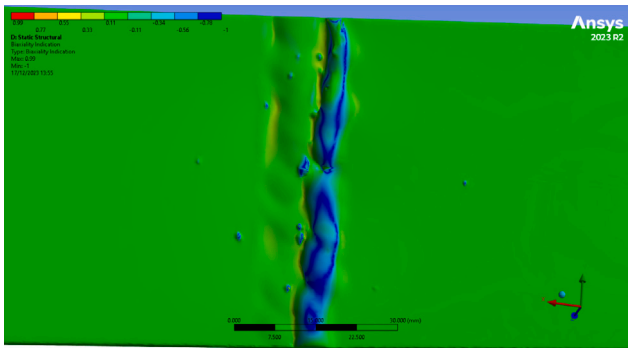

Fig. 9. Specimen No. 1 - Biaxiality indication.

when assessing the fatigue limit of the welded joint. By biaxiality indication definition (see Section 3.3), the corresponding range for biaxiality indication is $-0.38 \div 1$. In all the investigated specimens the biaxility indication was within the acceptable range. Where, as in Fig. 9 these values were lower than −0.38, they were located in protruding points and therefore not loaded. Actually, different defects could interact [60] and interaction can be more effective than the sum of each irregularity. Then, instead of considering the effect of each single irregularity orientation with respect to the load direction, a statistical approach of estimating the global effect of surface irregularity was applied.

4.3. On the crack nucleation

The results of the numerical simulation and 3D-life software were used to evaluate the crack nucleation sites. In Figs. 14–20 the minimum radius of curvature κ_{min} is plotted for each specimen and the red colored areas represent the areas where the radius lies in the threshold range.

The experimental fracture surfaces were therefore evaluated in order to point out the crack initiation sites, and those were compared with the simulation results (that is the most stressed points), and 3D-life indications (that is the points with the minimum radius of curvature). An example of crack initiation points on fracture surface for specimen no.3 is reported in Fig. 10.

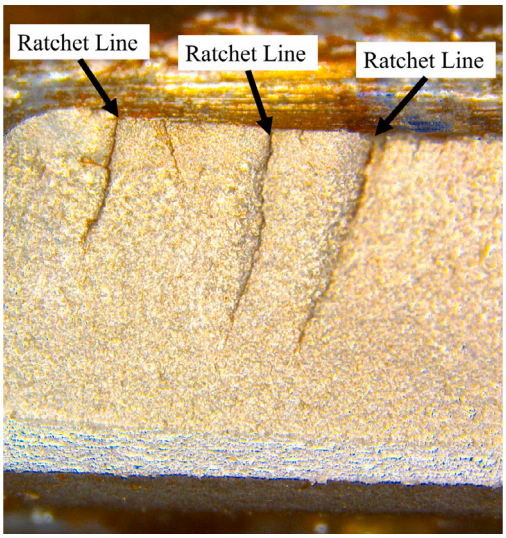

Fig. 10. Ratchet lines on fracture surface of specimen no.3.

The visual fracture analysis conducted on experimental samples revealed that many ratchet lines are present, pointing out that cracks originated from multiple points. In fact, the irregularities are evenly distributed in the surface and tend to interact between, and so several cracks generate. In some cases the crack crossed transversally the weld bead, showing how complex is the pattern of cracks that generate and propagate in the weld. This evidence corroborates the predictions made by the curvature-based algorithm. This methodology identifies the critical range of values of the radius of curvature where crack can nucleate due to irregularities notch effect. Furthermore, the algorithm maps their locations allowing the operator to correct/mitigate the notch effect due to irregularities. However, there is a need to clarify the relationship between these initiation points and the high-stress zones identified by the numerical simulation. The simulation suggested the most stressed point as the likely crack initiation site, despite its association with a low Fatigue Safety Factor (FSF). This discrepancy raises questions about the correlation between the predicted and actual initiation sites. In fact, crack initiation was found also in part with $FSF < 1$. However, since the simulated stresses are correlated to the curvature, the cracks initiated in the most stressed zones. This suggests that the fatigue limit of 160 MPa does not represent the actual behavior of the HAZ and the weld bead, that it is weaker. The curvature-based method shows the critical points for crack nucleation in the specimen; while the numerical solution relies on the material fatigue limit and the loading condition to estimate the 'not-safe' points. The curvature method highlighted several critical points on each specimen and experimental evidence of multiple distributed cracks confirmed this forecast. The numerical simulation was not able to predict multiple crack nucleation points.

In comparing the methodologies, it is noteworthy that the simulation method requires a predefined load to locate potential crack initiation sites, whereas the curvature-based approach does not rely on any pre-assumed load. The latter leverages the geometry of the weld bead itself, enabling the estimation of stress concentration locations without the need for external load information. This distinction is crucial for understanding the inherent capabilities and limitations of each method in predicting fracture initiation.

5. Conclusion

The traditional approach to the influence of notches in fatigue life of components is based on three main parameters: the stress intensity factor k_t related to geometry, the effective fatigue notch factor k_f and the notch sensitivity q both related to geometry and material. The k_t can be calculated according to theory of elasticity and most common notch shapes have tabulated stress intensity factor values. In the case of non-tabulated notches geometry, the stress distribution and the corresponding k_t can be obtained by means of FEM analysis. Then the fatigue safety factor can be obtained based on material data, available in software libraries. In the case of weldings, where material uncertainties and surface irregularity make these models inapplicable, an alternative procedure is required to propose reliable life estimation and fatigue safety factor, especially for manual welding.

In the present paper a k_f estimation model based on weld bead surface morphology is proposed. The presented approach includes the fundamentals of fatigue notch effect knowledge, implemented in a simple and low cost procedure. The paper investigates the relationship between fatigue life and the geometric parameters of weld bead surface. In particular a set of parameters related to local curvature in surface irregularities is defined. For each parameter, a Damage Index is defined to quantify the occurrence of irregularities on the weld bead surface. Specimens surfaces were scanned, and their weld beads surfaces were characterized. Then the specimens were tested by means of alternating testing fatigue. Empirical models were calibrated and validated relating the effective fatigue notch factor k_f vs the investigated local curvature parameters. Fatigue testing confirmed a notable scatter in fatigue endurance of welded specimens, emphasizing the inherent challenges posed by welding processes.

The influence of curvature parameters on fatigue life was a standout aspect of this research. For all subsets, SMAW specimen shows higher k_f with respect to GMAW specimens, and the two subsets group in different areas of the plots. The curvature related parameters are better fitted by the numerical model for the SMAW samples then for the GMAW ones The GMAW tests showed low scatter, the points are in fact grouped in a small area, and it is consequently difficult to find a pattern, however the Minimum Curvature Radius shows a clear trend both for the radius and the damage index plot. The gaussian curvature radius plot shows an appreciable trend. The fracture analysis conducted on experimental samples revealed that cracks originated from multiple points, confirming the predictions made by the curvature-based algorithm. This methodology identifies and maps the critical range of the radius of curvature where crack can nucleate on weld bead surface. The multiple cracks occur in sites where the traditional FSF is not able to identify a risk. Actually, the simulation method requires a predefined load to locate potential crack initiation sites, whereas the curvature-based approach is based only on surface morphology, enabling the estimation of stress concentration locations without the need for external load information. This distinction is crucial for understanding the inherent capabilities and limitations of each method in predicting fracture initiation. The aim of the authors in this research is to propose a standardized parameter related to surface geometry that can be used in industrial application, and then valid in generic loading condition. This approach is coherent with the Standard approach (eg. ISO 5817).

Curvature, particularly the Gaussian and the maximum ones, emerged as potential indicators of the notch effect in the welding process. The close grouping of data points for GMAW tests indicates a consistent performance, which can be instrumental in predicting the fatigue life in industrial applications. On the other hand, the higher k_f values of SMAW specimens suggest a different behavioral pattern, necessitating more tailored approaches when dealing with SMAW welds. In conclusion, this research underscores the importance of understanding the nuances of different welding techniques. The insights drawn from this study can pave the way for optimizing welding processes, ultimately leading to more durable and reliable welded joints in industrial settings.

CRediT authorship contribution statement

Raffaella Sesana: Formal analysis, Investigation, Resources, Supervision, Writing – original draft, Writing – review & editing. **Luca Santoro:** Formal analysis, Investigation, Methodology, Software, Visualization, Writing – original draft, Writing – review & editing.

Declaration of competing interest

The authors declare that they have no known competing financial interests or personal relationships that could have appeared to influence the work reported in this paper.

Data availability

No data was used for the research described in the article.

Appendix

See Figs. 11–20.

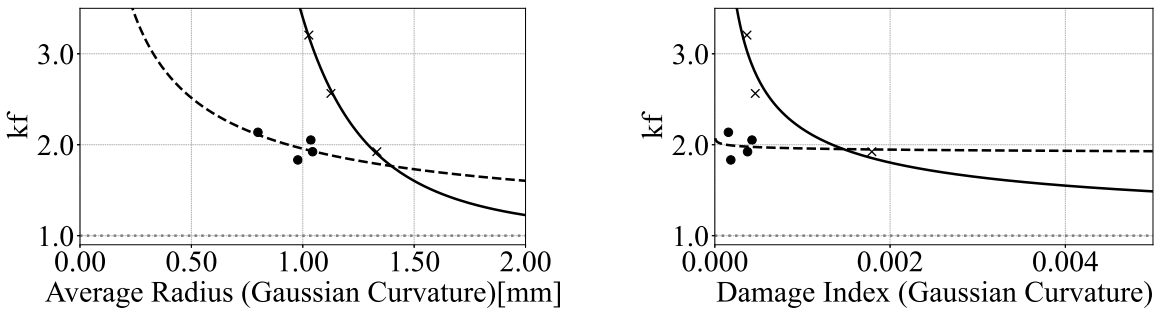

(a) radius (b) damage

Fig. 11. Experimental kf vs (a) Gaussian curvature and (b) Damage Index for SMAW ('*x*', continuous fitting curve) and GMAW ('*o*', dotted fitting curve) welds.

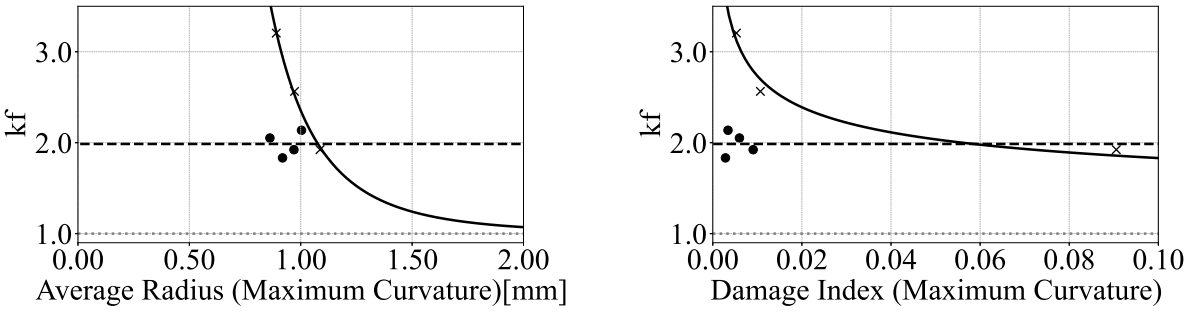

(a) radius (b) damage

Fig. 12. Experimental kf vs (a) Maximum curvature and (b) Damage Index for SMAW ('*x*', continuous fitting curve) and GMAW ('*o*', dotted fitting curve) welds.

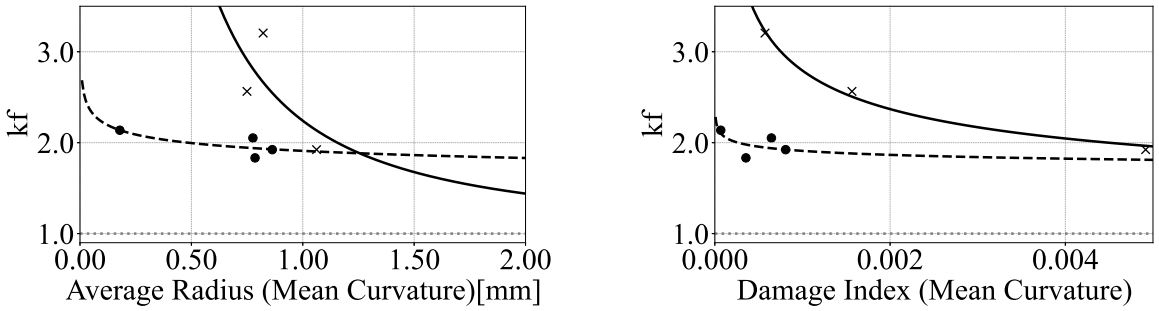

(a) radius (b) damage

Fig. 13. Experimental kf vs (a) Mean curvature and (b) Damage Index for SMAW ('*x*', continuous fitting curve) and GMAW ('*o*', dotted fitting curve) welds.

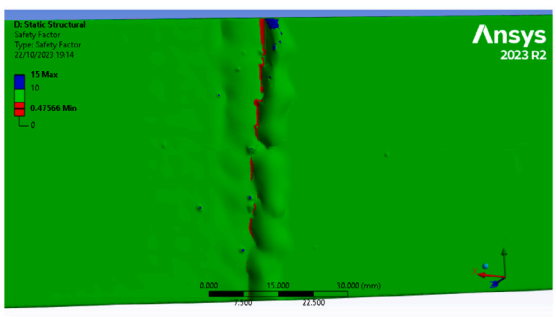

(a) Numerical FSF

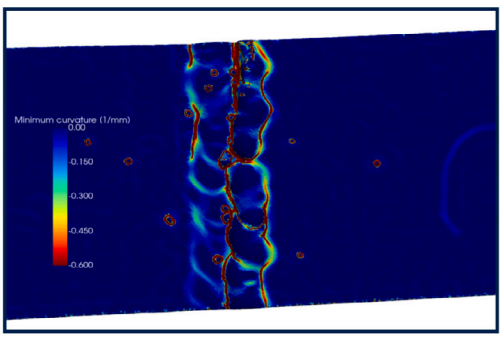

(b) κ_{min} plot

Fig. 14. Specimen no. 1.

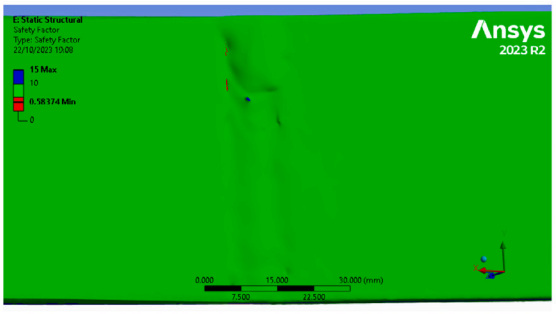

(a) Numerical FSF

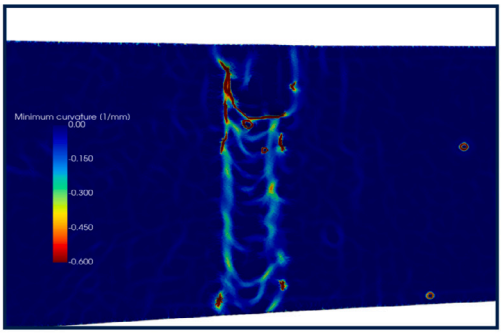

(b) κ_{min} plot

Fig. 15. Specimen no. 2.

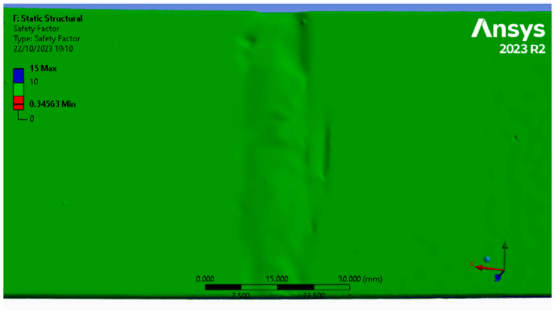

(a) Numerical FSF

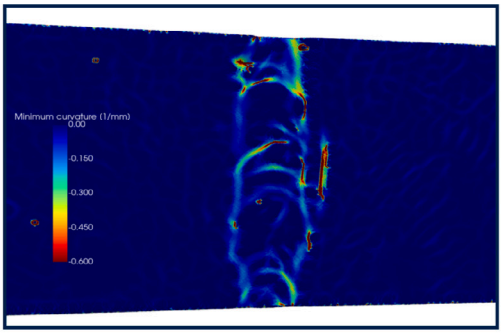

(b) κ_{min} plot

Fig. 16. Specimen no. 3.

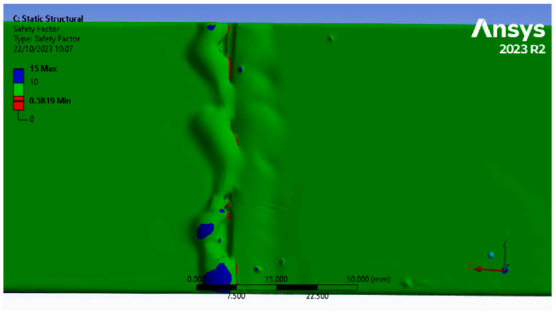

(a) Numerical FSF

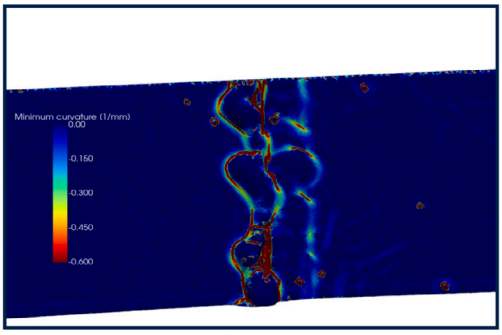

(b) κ_{min} plot

Fig. 17. Specimen no. 4.

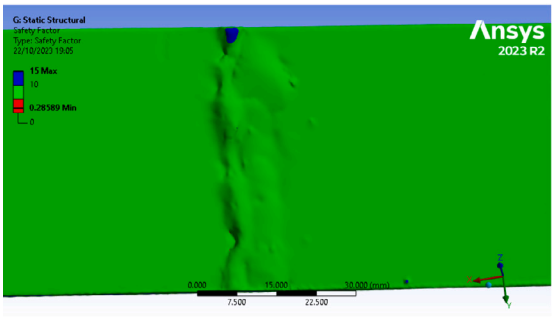

(a) Numerical FSF

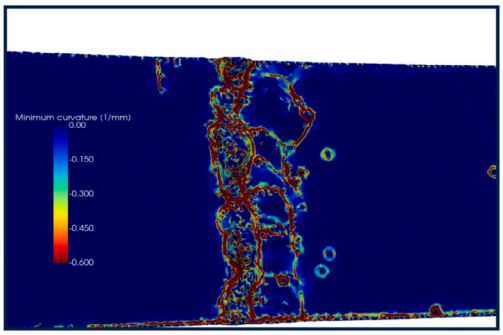

(b) κ_{min} plot

Fig. 18. Specimen no. 5.

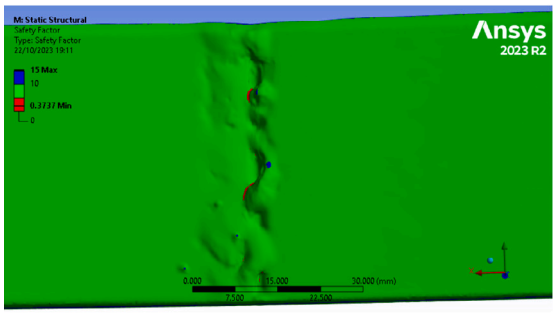

(a) Numerical FSF

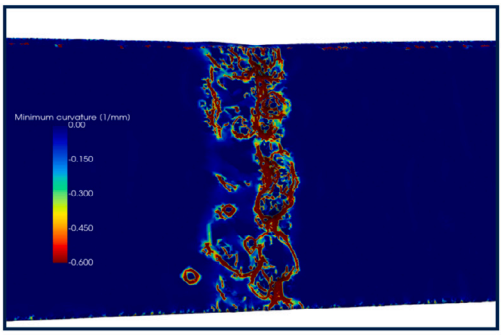

(b) κ_{min} plot

Fig. 19. Specimen no. 6.

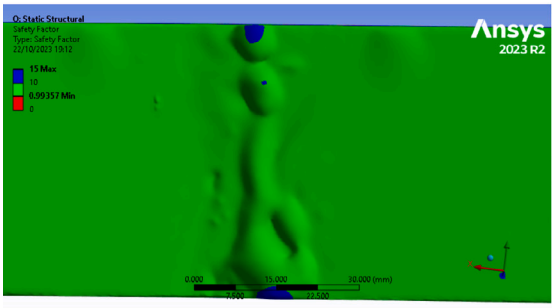

(a) Numerical FSF

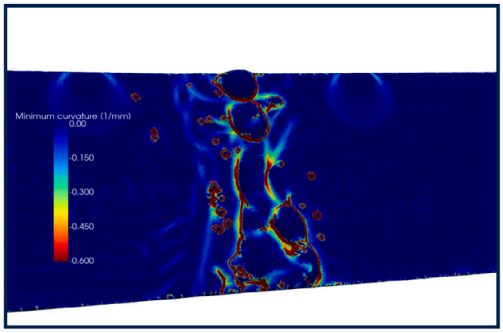

(b) κ_{min} plot

Fig. 20. Specimen no. 7.

References

[1] T. Aldeeb, M. Abduelmula, Fatigue strength of S275 mild steel under cyclic loading, World Acad. Sci. Eng. Technol. Int. J. Mater. Metall. Eng. 12 (10) (2018) 564–570, URL https://www.researchgate.net/publication/328355534.

[2] P. Lehto, J. Romanoff, H. Remes, T. Sarikka, Characterisation of local grain size variation of welded structural steel, Weld. World 60 (4) (2016) 673–688, http://dx.doi.org/10.1007/S40194-016-0318-8.

[3] H.L. Nguyen, A. Van Nguyen, H.L. Duy, T.H. Nguyen, S. Tashiro, M. Tanaka, Relationship among Welding Defects with Convection and Material Flow Dynamic Considering Principal Forces in Plasma Arc Welding, Metals 11 (9) (2021) 1444, http://dx.doi.org/10.3390/met11091444, URL https://www.mdpi.com/2075-4701/11/9/1444.

[4] L. Aucott, D. Huang, H.B. Dong, S.W. Wen, J.A. Marsden, A. Rack, A.C. Cocks, Initiation and growth kinetics of solidification cracking during welding of steel, Sci. Rep. 7 (2017) http://dx.doi.org/10.1038/srep40255, URL www.nature.com/scientificreports.

[5] C. Zhu, J. Cheon, X. Tang, S.J. Na, H. Cui, Molten pool behaviors and their influences on welding defects in narrow gap GMAW of 5083 Al-alloy, Int. J. Heat Mass Transfer 126 (2018) 1206–1221, http://dx.doi.org/10.1016/j.ijheatmasstransfer.2018.05.132.

[6] L. Santoro, R. Sesana, R. Molica Nardo, F. Curá, Infrared in-line monitoring of flaws in steel welded joints: a preliminary approach with SMAW and GMAW processes, Int. J. Adv. Manuf. Technol. (2023) http://dx.doi.org/10.1007/s00170-023-12044-2.

[7] D.W. Cho, S.J. Na, M.H. Cho, J.S. Lee, Simulations of weld pool dynamics in V-groove GTA and GMA welding, Weld. World 57 (2) (2013) 223–233, http://dx.doi.org/10.1007/s40194-012-0017-z.

[8] F. Mancini, H. Remes, J. Romanoff, P. Gallo, Influence of weld rigidity on the non-linear structural response of beams with a curved distortion, Eng. Struct. 246 (2021) http://dx.doi.org/10.1016/j.engstruct.2021.113044.

[9] C.M. Sonsino, Effect of residual stresses on the fatigue behaviour of welded joints depending on loading conditions and weld geometry, Int. J. Fatigue 31 (1) (2009) 88–101.

[10] S. Maddox, Fatigue Strength of Welded Structures, 2002, http://dx.doi.org/10.1016/c2013-0-17455-7, URL https://books.google.com/books?hl=it&lr=&id=e3FdDAAAQBAJ&oi=fnd&pg=PP1&ots=l_DF9wtNEV&sig=Wx-vYPzjroEyKdy7A_7H0MRdwlc.

[11] R. Sesana, L. Santoro, F. Curà, R. Molica Nardo, P. Pagano, Assessing thermal properties of multipass weld beads using active thermography: microstructural variations and anisotropy analysis, Int. J. Adv. Manuf. Technol. (2023) http://dx.doi.org/10.1007/s00170-023-11951-8.

[12] H. Neuber, Theory of stress concentration for shear-strained prismatical bodies with arbitrary nonlinear stress-strain law, J. Appl. Mech. Trans. ASME 28 (4) (1960) 544–550, http://dx.doi.org/10.1115/1.3641780.

[13] M. Kaffenberger, M. Vormwald, Considering size effects in the notch stress concept for fatigue assessment of welded joints, in: Computational Materials Science, Vol. 64, 2012, pp. 71–78, http://dx.doi.org/10.1016/j.commatsci.2012.02.047.

[14] A. Ghantasala, J. Diller, A. Geiser, D. Wenzler, D. Siebert, C. Radlbeck, R. Wüchner, M. Mensinger, K.U. Bletzinger, Node-Based Shape Optimization and Mechanical Test Validation of Complex Metal Components and Support Structures, Manufactured by Laser Powder Bed Fusion, in: Lecture Notes in Networks and Systems, vol. 274, Springer Science and Business Media Deutschland GmbH, 2021, pp. 10–17, http://dx.doi.org/10.1007/978-3-030-80462-6_2.

[15] Y. Murakami, Material defects as the basis of fatigue design, Int. J. Fatigue 41 (2012) 2–10, http://dx.doi.org/10.1016/j.ijfatigue.2011.12.001.

[16] U. Zerbst, M. Madia, C. Klinger, D. Bettge, Y. Murakami, Defects as a root cause of fatigue failure of metallic components. I: Basic aspects, in: Engineering Failure Analysis, Vol. 97, 2019, pp. 777–792, http://dx.doi.org/10.1016/j.engfailanal.2019.01.055.

[17] J. Diller, J. Blankenhagen, D. Siebert, C. Radlbeck, M. Mensinger, Combined Effect of Surface Treatment and Heat Treatment on the Fatigue Properties of AISI 316L, Manufactured by Powder Bed Fusion of Metals Using a Laser (PBF-LB/M).

[18] C.M. Sonsino, M. Kueppers, M. Eibl, G. Zhang, Fatigue strength of laser beam welded thin steel structures under multiaxial loading, Int. J. Fatigue 28 (5–6) (2006) 657–662, http://dx.doi.org/10.1016/j.ijfatigue.2005.09.013.

[19] A. Ahola, T. Björk, Z. Barsoum, Fatigue strength capacity of load-carrying fillet welds on ultra-high-strength steel plates subjected to out-of-plane bending, Eng. Struct. 196 (2019) http://dx.doi.org/10.1016/j.engstruct.2019.109282.

[20] W. Fricke, Recent developments and future challenges in fatigue strength assessment of welded joints, Proc. Inst. Mech. Eng. C 229 (7) (2015) 1224–1239, http://dx.doi.org/10.1177/0954406214550015.

[21] F. Berto, O. Fergani, A review of the notch rounding approach under in plane mixed mode loading, Int. J. Fatigue 101 (2017) 127–136.

[22] F. Berto, P. Lazzarin, Multiparametric full-field representations of the in-plane stress fields ahead of cracked components under mixed mode loading, Int. J. Fatigue 46 (2013) 16–26, http://dx.doi.org/10.1016/j.ijfatigue.2011.12.004.

[23] Š. Kalač, M. Mensinger, C. Radlbeck, N. Zejnelagić, Đ. Đuričić, D. Lučić, Experimental and Theoretical Research on Welded Aluminum K-Joints, in: Engineering Proceedings 2023, Vol. 43, No. 1, Multidisciplinary Digital Publishing Institute, 2023, p. 18, http://dx.doi.org/10.3390/engproc2023043018, https://www.mdpi.com/2673-4591/43/1/18/htm https://www.mdpi.com/2673-4591/43/1/18.
[24] T. Nykänen, T. Björk, Assessment of fatigue strength of steel butt-welded joints in as-welded condition - Alternative approaches for curve fitting and mean stress effect analysis, Mar. Struct. 44 (2015) 288–310, http://dx.doi.org/10.1016/j.marstruc.2015.09.005.
[25] K. Yokoyama, C. Miki, Participatory database of repair cases on fatigue damaged welded structures, Int. J. Fatigue 101 (2017) 385–396, http://dx.doi.org/10.1016/j.ijfatigue.2017.01.010.
[26] M. Braun, A. Ahola, A.S. Milaković, S. Ehlers, Comparison of local fatigue assessment methods for high-quality butt-welded joints made of high-strength steel, Forces Mech. 6 (November) (2022) 100056, http://dx.doi.org/10.1016/j.finmec.2021.100056, URL https://www-sciencedirect-com.ezproxy.biblio.polito.it/science/article/pii/S2666359721000470.
[27] I. Lillemäe, H. Lammi, L. Molter, H. Remes, Fatigue strength of welded butt joints in thin and slender specimens 44, 2012, pp. 98–106, http://dx.doi.org/10.1016/j.ijfatigue.2012.05.009.
[28] H. Remes, P. Varsta, Statistics of weld geometry for laser-hybrid welded joints and its application within notch stress approach 54(7–8), 2010, pp. R189–R207.
[29] T. Lassen, N. Recho, Proposal for a more accurate physically based S-N curve for welded steel joints, Int. J. Fatigue 31 (1) (2009) 70–78, http://dx.doi.org/10.1016/J.IJFATIGUE.2008.03.032.
[30] G. Meneghetti, A. Campagnolo, A. Visentin, Automated fatigue strength assessment of arc-welded structures according to the peak stress method, Procedia Struct. Integr. 28 (2020) 1062–1083, http://dx.doi.org/10.1016/j.prostr.2020.11.122.
[31] Y.K. Park, J.G. Shin, Fatigue strength evaluation of a welded structure by a concentrated load close to the welded joint, J. Mech. Sci. Technol. 31 (4) (2017) 1789–1796, http://dx.doi.org/10.1007/s12206-017-0326-7.
[32] G. Meneghetti, A. Campagnolo, State-of-the-art review of peak stress method for fatigue strength assessment of welded joints, Int. J. Fatigue 139 (2020) http://dx.doi.org/10.1016/j.ijfatigue.2020.105705.
[33] G. Meneghetti, A. Campagnolo, F. Berto, Fatigue strength assessment of partial and full-penetration steel and aluminium butt-welded joints according to the peak stress method, Fatigue Fract. Eng. Mater. Struct. 38 (12) (2015) 1419–1431, http://dx.doi.org/10.1111/ffe.12342.
[34] G. Meneghetti, P. Lazzarin, Significance of the elastic peak stress evaluated by FE analyses at the point of singularity of sharp V-notched components, Fatigue Fract. Eng. Mater. Struct. 30 (2) (2007) 95–106, http://dx.doi.org/10.1111/j.1460-2695.2006.01084.x.
[35] C. Delprete, L.G.D. Maggio, R. Sesana, Theory of critical distances: A discussion on concepts and applications, Proc. Inst. Mech. Eng. C 235 (21) (2021) 5695–5708, http://dx.doi.org/10.1177/0954406220985887.
[36] J. Said, S. Garcin, S. Fouvry, G. Cailletaud, C. Yang, F. Hafid, A Multi-Scale Strategy to Predict Fretting-Fatigue Endurance of Overhead Conductors.
[37] B. Vayssette, N. Saintier, C. Brugger, M. Elmay, E. Pessard, Surface roughness of Ti-6Al-4V parts obtained by SLM and EBM: Effect on the High Cycle Fatigue life, in: Procedia Engineering, Vol. 213, 2018.
[38] Y. Wu, B. Gao, J. Zhao, Y. Wang, Z. Liu, J. Chen, Y. Ying, G.Y. Tian, Weld crack detection based on region electromagnetic sensing thermography, IEEE Sens. J. 19 (2) (2019) 751–762, http://dx.doi.org/10.1109/JSEN.2018.2868867.
[39] I. Al Zamzami, L. Susmel, On the accuracy of nominal, structural, and local stress based approaches in designing aluminium welded joints against fatigue, Int. J. Fatigue 101 (2017) 137–158, http://dx.doi.org/10.1016/j.ijfatigue.2016.11.002.
[40] J. Baumgartner, H.C. Yıldırım, Z. Barsoum, Fatigue strength assessment of TIG-dressed welded steel joints by local approaches, Int. J. Fatigue 126 (2019) 72–78, http://dx.doi.org/10.1016/j.ijfatigue.2019.04.038.
[41] K. Lipiäinen, A. Ahola, T. Björk, Fatigue performance of ultra-high-strength steel laser cut notches under variable amplitude loading, Weld. World 67 (9) (2023) 2235–2245, http://dx.doi.org/10.1007/S40194-023-01544-0.
[42] D. Taylor, D. Hoey, High cycle fatigue of welded joints: The TCD experience, Int. J. Fatigue 31 (1) (2009) 20–27, http://dx.doi.org/10.1016/j.ijfatigue.2008.01.011.
[43] Z. Hu, F. Berto, Y. Hong, L. Susmel, Comparison of TCD and SED methods in fatigue lifetime assessment, Int. J. Fatigue 123 (2019) 105–134, http://dx.doi.org/10.1016/j.ijfatigue.2019.02.009.
[44] I. Lillemäe, S. Liinalampi, H. Remes, A. Itävuo, A. Niemelä, Fatigue strength of thin laser-hybrid welded full-scale deck structure, Int. J. Fatigue 95 (2017) 282–292, http://dx.doi.org/10.1016/j.ijfatigue.2016.11.012.
[45] Y. Verreman, N. Limodin, Fatigue notch factor and short crack propagation, Eng. Fract. Mech. 75 (6) (2008) 1320–1335, http://dx.doi.org/10.1016/J.ENGFRACMECH.2007.07.005.
[46] International Organization for Standardization, BS EN ISO 5817:2023 Welding - Fusion-welded joints in steel, nickel, titanium and their alloys (beam welding excluded) - Quality levels for imperfections, 2023, pp. 1–26.
[47] S. Bhardwaj, R.M. Ratnayake, A. Keprate, Review of Weld Quality Classification Standard and Post Weld Fatigue Life Improvement Methods for Welded Joints, in: Lecture Notes in Civil Engineering, vol. 110, Springer Science and Business Media Deutschland GmbH, 2021, pp. 257–270, http://dx.doi.org/10.1007/978-981-15-9121-1_20.
[48] A. Niederwanger, D.H. Warner, G. Lener, The utility of laser scanning welds for improving fatigue assessment, Int. J. Fatigue 140 (2020) http://dx.doi.org/10.1016/j.ijfatigue.2020.105810.
[49] S. Shojai, P. Schaumann, M. Braun, S. Ehlers, Influence of pitting corrosion on the fatigue strength of offshore steel structures based on 3D surface scans, Int. J. Fatigue 164 (2022) http://dx.doi.org/10.1016/J.IJFATIGUE.2022.107128.
[50] J. Schubnell, M. Jung, C.H. Le, M. Farajian, M. Braun, S. Ehlers, W. Fricke, M. Garcia, A. Nussbaumer, J. Baumgartner, Influence of the optical measurement technique and evaluation approach on the determination of local weld geometry parameters for different weld types, Weld. World 64 (2) (2020) 301–316, http://dx.doi.org/10.1007/s40194-019-00830-0, URL https://link.springer.com/article/10.1007/s40194-019-00830-0.
[51] F. Renken, R.U.F. von Bock und Polach, J. Schubnell, M. Jung, M. Oswald, K. Rother, S. Ehlers, M. Braun, An algorithm for statistical evaluation of weld toe geometries using laser triangulation, Int. J. Fatigue 149 (2021) http://dx.doi.org/10.1016/j.ijfatigue.2021.106293.
[52] J. Schubnell, S.K. Konidena, M. Jung, M. Braun, S. Ehlers, M. Madia, T. Kannengießer, D. Löschner, Approach for the probabilistic fatigue assessment of welded joints based on the local geometry of the weld seam, Fatigue Fract. Eng. Mater. Struct. (2023) http://dx.doi.org/10.1111/FFE.14170, URL https://onlinelibrary.wiley.com/doi/10.1111/ffe.14170.
[53] ASTM, ASTM E1823 13 Standard Terminology Relating to Fatigue and Fracture Testing, ASTM International, 100 Barr Harbor Drive, PO Box C700, West Conshohocken, PA 19428-2959. United States, 2013.
[54] European Committee for Standardization, EN ISO 6507–1 (2018) Standards Publication Metallic materials - Vickers hardness test, 2018, URL https://bsol.bsigroup.com/.
[55] S. Concentration, T. Edition, W.D. Pilkey, D.F. Pilkey, Peterson ' S Stress Peterson ' S Stress Concentration, 2008.
[56] M. Khurshid, Z. Barsoum, I. Barsoum, T. Däuwel, The multiaxial weld root fatigue of butt welded joints subjected to uniaxial loading, Fatigue Fract. Eng. Mater. Struct. 39 (10) (2016) 1281–1298, http://dx.doi.org/10.1111/ffe.12444.
[57] J.E. Shigley, R.G. Budynas, J.K. Nisbett, Progetto e costruzione di macchine 1, 2013.
[58] H.W. McKenzie, D.J. White, Stress concentration caused by an oblique round hole in a flat plate under uniaxial tension, J. Strain Anal. Eng. Des. 3 (2) (1968) 98–102, http://dx.doi.org/10.1243/03093247V032098.
[59] I.M. Daniel, Photoelastic analysis of stresses around oblique holes, Exp. Mech. 10 (11) (1970) 467–473, http://dx.doi.org/10.1007/bf02327674.
[60] A.F. Hobbacher, Recommendations for Fatigue Design of Welded Joints and Components, 2019, p. E3, http://dx.doi.org/10.1007/978-3-319-23757-2_8, URL http://www.springer.com/series/13906.